Field-Induced Ferromagnetic Metallic State of Bilayer Manganite $(La_{0.4}Pr_{0.6})_{1.2}Sr_{1.8}Mn_2O_7$: A Polarized Neutron Diffraction Study

F. Wang,[1] A. Gukasov,[1] F. Moussa,[1] M. Hennion,[1] M. Apostu,[2] R. Suryanarayanan,[2] and A. Revcolevschi[2]
[1]*Laboratoire Léon Brillouin (CEA-CNRS), CE Saclay, 91191 Gif sur Yvette, France*
[2]*Laboratoire de Physico-Chimie de l'Etat Solide, Université Paris-Sud, 91405, Orsay, France*
(Received 5 February 2003; published 25 July 2003)

Unpolarized and polarized neutron diffraction measurements have been carried out on the bilayer manganite $(La_{0.4}Pr_{0.6})_{1.2}Sr_{1.8}Mn_2O_7$ which undergoes simultaneous semiconductor-metal paraferromagnetic transitions under magnetic field. Maximum entropy magnetization density reconstruction and multipole refinement on flipping ratios evidence the existence of two distinct field-induced states. The field-induced ferromagnetic state where the field is parallel to the c axis is characterized by the presence of magnetic moment on the Sr site of $0.48(2)\mu_B$, due to the Pr substitution. It also shows a high population of the $d_{3z^2-r^2}$ orbitals of Mn^{3+}. For the field-induced state where the field is parallel to the a or b axes no magnetization density was found at the Sr site and the $d_{x^2-y^2}$ orbital is slightly more populated than the $d_{3z^2-r^2}$ one.

DOI: 10.1103/PhysRevLett.91.047204 PACS numbers: 75.25.+z, 75.50.Cc, 75.50.Gg

Though the colossal magnetoresistance (CMR) and other properties such as charge ordering exhibited by the manganese perovskites have been extensively investigated, there has been no quantitative theoretical model to account for all of these properties [1]. However, it is generally accepted that these varied properties are a result of the manifestation of the orbital degree of freedom of the e_g electrons. More recently, the double layer manganites $La_{2-2x}Sr_{1+2x}Mn_2O_7$ ($x = 0$–0.5) have attracted much attention [2,3], not only because of a CMR reaching 98% for $x = 0.4$ ($T_c = 125$ K) but also due to the highly anisotropic properties arising from the 2D structure in contrast with the cubic perovskites. Further, it was recently shown [4] that the Pr-substituted compound, $(La_{0.4}Pr_{0.6})_{1.2}Sr_{1.8}Mn_2O_7$, did not show any spontaneous magnetic ordering but, on an application of a field of 5 T parallel to the c axis, exhibited a first-order paraferromagnetic transition, with the resistance along the c axis reduced by a factor of 10^6 at 5 K. This was accompanied by a large negative magnetostriction. Further, below 50 K, an anisotropic magnetic memory effect was observed [5] in which both resistivity and magnetization were magnetic history dependent. These were thought to arise from field-induced changes in the occupancy of the e_g electrons. However, no microscopic evidence has been found so far to explain this. To elucidate this phenomenon further, we have carried out extensive polarized neutron diffraction (PND) measurements on a single crystal sample of $(La_{0.4}Pr_{0.6})_{1.2}Sr_{1.8}Mn_2O_7$.

PND is an extremely powerful tool to study magnetization densities in crystals. It provides direct information on the distribution of the magnetization at different crystallographic sites of the unit cell, their local anisotropy, and also allows separation of the spin and orbital contributions to magnetic moments. In favorable cases, PND further allows one to determine the symmetry of occupied orbitals [6,7]. Although PND does not measure the orbital occupancies directly, it gives information about the unpaired electron density, which can be compared to the theory predictions for the Mn^{3+} orbital configuration.

Neutron diffraction studies were performed at the ORPHÉE 14 MW reactor of the Léon Brillouin Laboratory, CEA/CNRS Saclay. Integrated intensities of Bragg reflections were collected on the lifting-counter diffractometer 6T2, with the 7.5 T cryomagnet using unpolarized neutrons of wavelength $\lambda_n = 0.90$ Å. Polarized neutron flipping ratios were measured on the lifting-counter diffractometer 5C1 using neutrons with $\lambda_n = 0.84$ Å obtained with a Heusler alloy monochromator, with polarization of the incident neutron beam $P_0 = 0.91$. The programs SORGAM and MPLSQ of the Cambridge Crystallography Subroutine Library [8] were used for the calculation of magnetic amplitudes and for the least squares refinements on the signed magnetic structure factors, respectively.

A single crystal of $(La_{0.4}Pr_{0.6})_{1.2}Sr_{1.8}Mn_2O_7$ was grown from a sintered rod of the same nominal composition by the floating-zone technique, using a mirror furnace [4]. Prior to polarized neutron measurements the crystal was characterized by neutron diffraction at 180 and 2 K in the zero-field cooled state. No additional intensity was found at 2 K, which confirms the absence of the magnetic ordering in the zero-field cooled state. Therefore the refinement of the crystal structure was performed using space group *I4/mmm*. The refinement has shown that, as in the parent (Pr-free) compound $La_{1.2}Sr_{1.8}Mn_2O_7$ [9], the bond lengths of O1 shared by two Mn ions are shorter [Mn-O1 = 1.955(5) Å] than that of the O2 [Mn-O2 = 2.017(5) Å] ionically coordinated by one Mn and one La(Pr,Sr) atom. The distortion of MnO_6 octahedra $\delta_{JT} = (d_{\text{Mn-O1}} + d_{\text{Mn-O2}})/2d_{\text{Mn-O3}} = 1.028(3)$ is slightly larger than that of the parent compound $La_{1.2}Sr_{1.8}Mn_2O_7$ and comparable to the distortion of the lightly hole-doped $La_{1.4}Sr_{1.6}Mn_2O_7$ [9–11].

The magnetization of our $(La_{0.4}Pr_{0.6})_{1.2}Sr_{1.8}Mn_2O_7$ crystal was measured directly by neutron diffraction. Before each measurement the sample was zero-field cooled from room temperature. Then the magnetic field was increased from 0 to 7 T, lowered to -7 T, and raised back to 7 T at a sweep rate of 100 mT per min, while the peak intensity of the (110) reflection was simultaneously recorded. Figures 1(a) and 1(c) show the field dependencies of the intensity of the (110) reflection at 2 K, with the field applied parallel to the $[\bar{1}10]$ and the [001] direction, respectively. (In both cases, the field-independent nuclear part of the scattering intensity was subtracted.) The jumps of intensities corresponding to the first-order phase transition from the magnetically disordered state to the field-induced ferromagnetic (FIFM) state are clearly seen in the figure. Several important features of the intensity curves are to be noted. First, the critical field for the in-plane magnetization, $H_{ab} = 6.1$ T, is about 20% higher than that for the out-of-plane magnetization, $H_c = 5.0$ T, which confirms the anisotropy of the FIFM state reported earlier [4]. Second, upon removing the field the intensity does not return to its original zero-field value for either field orientation. Third, the remanent intensity at $H = 0$ is very high for the in-plane field and relatively small for the out-of-plane one. The measured neutron intensities can be easily converted into conventional field-magnetization curves by scaling over a well known nuclear scattering structure factor of the (110) reflection and the theoretical magnetic form factor of Mn^{3+} ion [see Figs. 1(b) and 1(d)]. This procedure yields the remanent magnetization $1.1\mu_B$ and $3.0\mu_B$ per Mn atom for the in-plane and the out-of-plane field, respectively. We note as well that the out-of-plane saturation magnetization $M_c = 3.8\mu_B$ is 20% higher than the in-plane magnetization $M_{ab} = 3.2\mu_B$, in agreement with [4]. Thus, depending on field orientation, two different FIFM states can be obtained, both being stable upon removing the field but having different remanent magnetizations. At 2 K, the relaxation time of both states was too large to be measured by neutron scattering; however, the original nonmagnetic state could be recovered by heating the crystal above 34 K. Finally, the critical field value H_a, measured with the field along the [100] direction, was found to be the same as H_{ab}, indicating that the anisotropy within the tetragonal plane can be neglected.

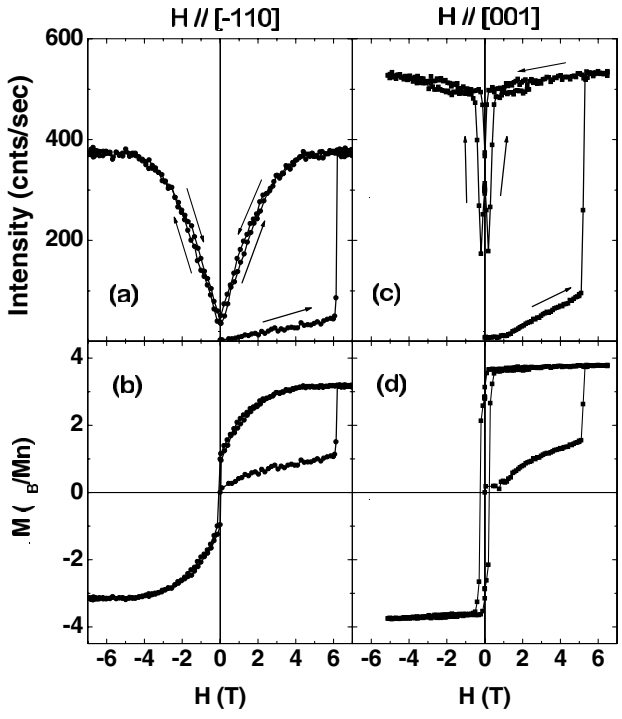

FIG. 1. Field-induced neutron scattering intensity of the (110) reflection at 2 K: (a) H parallel to the $[\bar{1}10]$ direction, (c) $H \parallel [001]$. Magnetization deduced from the scattering intensity of the (110) reflection: (b) H parallel to the $[\bar{1}10]$ direction, (d) H parallel to [001].

To clarify the difference between two FIFM states, three sets of polarized neutron flipping ratios were measured at 2 K. First, a field of 6.5 T (higher than the critical field $H_{ab} = 6.1$ T) was applied parallel to the $[\bar{1}10]$ direction on the zero-field cooled sample and 116 (68 independent) flipping ratios were measured. Second, the same procedure was applied for $H \parallel [100]$ giving 179 (59) flipping ratios. We considered that in both cases the sample was in the same FIFM(ab) state and two sets have been merged in the data treatment. The third set of 174 (73) flipping ratios was measured in the FIFM(c) state, which was created by an application of a magnetic field of 5.5 T along the [001] direction. Since this state is characterized by a lower critical field $H_c = 5$ T and a higher saturation (and remanent) magnetization, these data were treated separately. For comparison the same sets of flipping ratios were also measured just below the critical field of the FIFM transition, namely, at $H = 5.0$ T for the [100], $[\bar{1}10]$ directions and at $H = 4.5$ T for the [001] one.

The magnetic amplitudes $f_M(\mathbf{Q})$ of all measured reflections were obtained using the SORGAM [8] program. They are shown in Fig. 2 together with the theoretical magnetic form factor of the Mn^{3+} ion. (For convenience, the amplitudes were normalized by the geometrical structure factor for the Mn atoms $[4\cos(2\pi l z_{\mathrm{Mn}})]$. If all the magnetization $\mathbf{M}(\mathbf{Q})$ is associated with the Mn site and is distributed spherically, one should expect $f_M(\mathbf{Q})$ to be a smooth function of $\mathbf{Q}$.

As seen from Fig. 2(a), where the amplitudes for the in-plane FIFM state are shown, the majority of the measured magnetic amplitudes lies reasonably close to the theoretical curve. On the contrary, for the out-of-plane FIFM state [Fig. 2(b)] the amplitudes of many reflections, especially those at low $\mathbf{Q}$, deviate strongly from the theoretical function. This usually indicates that a considerable amount of the moment is delocalized from the Mn site to some other position.

To localize the position and the magnitude of this additional density we used a model-free analysis of our

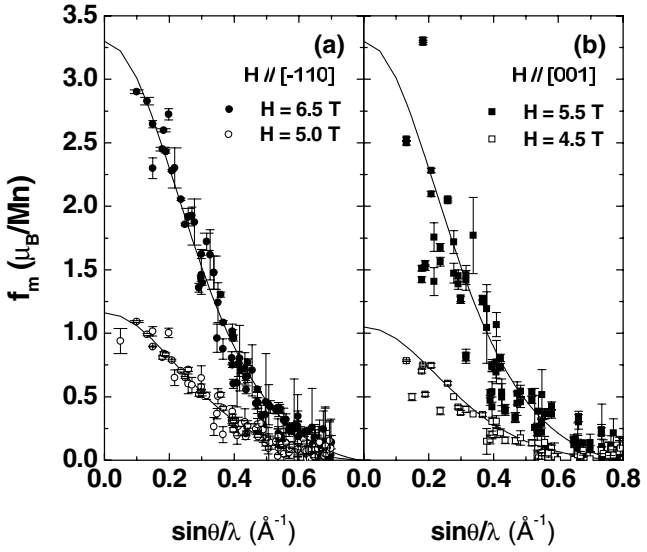

FIG. 2. The magnetic amplitudes per Mn atom in $(La_{0.4}Pr_{0.6})_{1.2}Sr_{1.8}Mn_2O_7$ at 2 K: (a) magnetic field in the *ab* plane: open circles $H = 5.0$ T; filled circles $H = 6.5$ T [FIFM(*ab*) state]. (b) Field perpendicular to the *ab* plane: open squares $H = 4.5$ T; filled squares $H = 5.5$ T [FIFM(*c*) state]. The solid lines are the Mn^{3+} form factor scaled to $1.1\mu_B$ and $3.3\mu_B$ for the low- and high-field data, respectively.

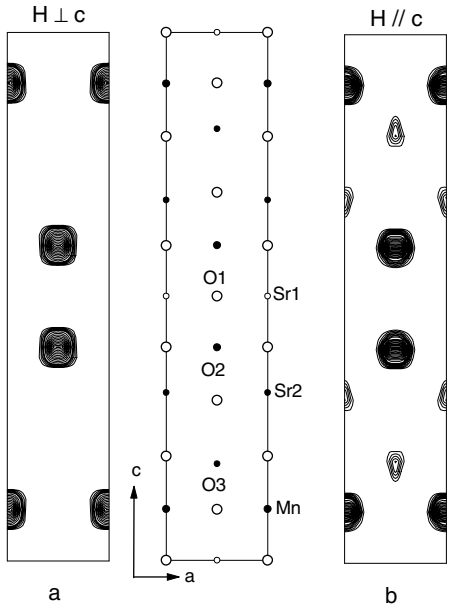

FIG. 3. Maximum entropy reconstruction of the magnetization distribution in $(La_{0.4}Pr_{0.6})_{1.2}Sr_{1.8}Mn_2O_7$ at 2 K. The maps show the projections of the magnetization density on the [100] direction: *a* for a magnetic field of 6.5 T in the *ab* plane [FIFM(*ab*) state] and *b* for a magnetic field of 5.5 T perpendicular to the *ab* plane [FIFM(*c*) state]. The contour step is $0.2\mu_B$.

data based on the reconstruction of the 3D magnetization distribution using the maximum entropy method (MEM). This method has been shown to give more reliable results than conventional Fourier syntheses, by considerably reducing both noise and truncation effects [12–14].

Figures 3(a) and 3(b) show the magnetic density distributions of our crystal for the in-plane FIFM(*ab*) and the out-of-plane FIFM(*c*) state, respectively. As seen from Fig. 3(a), the magnetization density of the FIFM(*ab*) state is concentrated only at the Mn sites. On the contrary the FIFM(*c*) state, apart from the Mn spin density, exhibits a very substantial density at the Sr2 site [see Fig. 3(b)]. The total moment present at the Sr2 site is more than 15% of the total magnetization density and can be estimated as $0.5\mu_B$–$0.6\mu_B$ per Sr2 site. The magnetic moment can be attributed to the Pr atoms substituting Sr (or La) and appears only when the magnetic field is applied parallel to the *c* axis. Taking into account the occupancy factor of Pr (0.24), we can estimate the average moment induced on Pr atoms as $2\mu_B$.

Similar analysis performed for the zero-field cooled semiconducting states in the fields $H = 4.5$ T $\parallel [001]$ and $H = 5.5$ T $\parallel [\bar{1}10]$, below their critical values, gives qualitatively similar results. In both cases the moment induced at the Mn site was found to be equal to $1.1\mu_B$. No Pr moment was found for $H \parallel ab$ and $0.3\mu_B$ was found for $H \parallel c$. This shows a very strong anisotropy of the local susceptibility parameters of Sr2 [15], which is probably due to the uniaxial (tetragonal) symmetry of its local environment. Thus, two FIFM states of $(La_{0.4}Pr_{0.6})_{1.2}Sr_{1.8}Mn_2O_7$, characterized by different magnetic and transport properties, are microscopically different and can be distinguished by the presence (the absence) of the induced moment on the Pr occupying the Sr2 site. We note that MEM does not show any magnetic moment at the Sr1 site.

Further analysis of the measured flipping ratios was performed by refinement. First we used a spherical model in which both spin and orbital contributions to the *3d* Mn moments were allowed. For this purpose the series expansion of the form factors of Mn^{3+} in the dipole approximation was used: $\mu f(Q) = (\mu_S + \mu_L)\langle j_0\rangle + \mu_L\langle j_2\rangle$ [8]. As seen from Table I this simple model works quite well for the FIFM(*ab*) state and gives relatively good (low) agreement indices ($\chi^2 = 7.42$ and $R_w = 6.1\%$). (We note that neglecting the orbital part of the Mn form factor deteriorates the quality of the fit considerably, indicating that the orbital part of the Mn moment exists and should be taken into account.) On the contrary, the model with only two parameters of Mn fails to describe the FIFM(*c*) state; $\chi^2 = 54.4$ and $R_w = 32\%$.

In the second model a spherically distributed moment described by the radial functions $\langle j_0\rangle$ and $\langle j_2\rangle$ of Pr^{3+} around the SR2 position was allowed. These additional parameters do not change the agreement factors for the FIFM(*ab*) state (see Table I) but improve drastically the fit quality for the out-of-plane FIFM(*c*) one, $\chi^2 = 10.9$ and $R_w = 13.2\%$. One can see that the fit shows the presence of a considerable amount of magnetic moment, $0.48(2)\mu_B$, at the SR2 site. This moment amounts to more

TABLE I. Results of refinement on signed magnetic structure factors deduced from the polarized neutron flipping ratios collected on the $(La_{0.4}Pr_{0.6})_{1.2}Sr_{1.8}Mn_2O_7$ at 2 K in magnetic fields of 6.5 and 5.5 T, applied perpendicular and parallel to the c axis, respectively. The values of all variables are given in Bohr magnetons per atom.

Data set	$H = 6.5$ T $\parallel ab$	$H = 5.5$ T $\parallel c$
No. of observ.	295	174
Spherical model: two variables		
χ^2	7.42	54.4
R_w	6.1	32.2
Mn $(\mu_S + \mu_L)\langle j_0\rangle$	3.32(2)	2.9(1)
Mn $\mu_L\langle j_2\rangle - 0.38(5)$	−0.6(2)	
Spherical model: four variables		
χ^2	7.42	10.9
R_w	6.0	13.2
Mn $(\mu_S + \mu_L)\langle j_0\rangle$	3.32(2)	2.9(1)
Mn $\mu_L\langle j_2\rangle$	−0.38(5)	−0.6(2)
Sr2 $(\mu_S + \mu_L)\langle j_0\rangle$	0.00(2)	0.48(2)
Sr2 $\mu_L\langle j_2\rangle$	−0.01(2)	0.77(4)
Multipole model		
χ^2	4.20	5.68
R_w	4.3	8.8
Mn $Y_{00}\langle j_0\rangle$	**3.36(3)**	**3.12(5)**
Mn $Y_{20}\langle j_2\rangle$	0.03(2)	0.01(5)
Mn $Y_{44+}\langle j_4\rangle$	−0.18(9)	**−0.35(6)**
Mn $Y_{40}\langle j_4\rangle$	**−0.50**(7))	0.1(1)
Mn $\mu_L\langle j_2\rangle$	**−0.48(4)**	**−0.58(7)**
Sr2 $(\mu_S + \mu_L)\langle j_0\rangle$	···	**0.50(3)**
Sr2 $\mu_L\langle j_2\rangle$	···	**0.77(4)**
O1 $Y_{00}\langle j_0\rangle$ **0.15(2)**	−0.3(1)	
O2 $Y_{00}\langle j_0\rangle$	0.03(2)	-0.2(1)
O3 $Y_{00}\langle j_0\rangle$	−0.05(1)	0.05(5)
Orbital occupancies from multipole model (%)		
Mn $d_{x^2-y^2}$	14(3)	9(4)
Mn $d_{3z^2-r^2}$	11(3)	20(4)
Mn d_{xy}	23(3)	30(4)
Mn d_{zx+zy}	52(3)	41(4)

than 15% of that of Mn in agreement with the MEM results.

In the third model the Mn density was modeled by a sum of spherical harmonic multipole functions allowed by the site symmetry *(4mm)*. The presence of a spherically distributed moment around the three oxygen sites was also allowed. The results given in Table I show a considerable improvement (by a factor of 2 for χ^2) of the agreement indices for the third model. We should note that not all of the six additional parameters have the same impact on the agreement factors. For example, only two of the parameters, Mn Y_{40} and O1 Y_{00}, give any significant improvement to the fit to the FIFM(ab) state, while the others have little influence on the fit quality. The same is valid for the FIFM(c) state. In fact, the Mn Y_{44+} alone accounts for more than half of the χ^2 decrease. To stress this point, the parameters which are essential for the refinement are written in bold characters in Table I.

The final block of Table I shows the occupancies of the *3d* orbitals of Mn derived from the refined multipole parameters. One can see that, as in the parent compound [7], the majority of spin, 70(8)%, at the Mn site arises from the t_{2g} electrons in both FIFM states. As with the e_g electons, we found that for the FIFM(ab) state the $d_{x^2-y^2}$ orbital occupation is slightly higher than that of the $d_{3z^2-r^2}$ one. On the contrary, the FIFM(c) state is characterized by the preferential occupation of the $d_{3z^2-r^2}$ orbital over the $d_{x^2-y^2}$ one.

In conclusion, PND demonstrates the existence of two different field-induced metastable states in $(La_{0.4}Pr_{0.6})_{1.2}Sr_{1.8}Mn_2O_7$. The FIFM($c$) state ($H \parallel c$) is characterized by the presence of a moment on the Sr site of $0.48(2)\mu_B$, due to the Pr substitution. It also shows a high population of the $d_{3z^2-r^2}$ orbitals of Mn^{3+}. For the FIFM(ab) state ($H \parallel a, b$), no magnetization density was found at the Sr site and the $d_{x^2-y^2}$ orbital is slightly more populated than the $d_{3z^2-r^2}$ one. Thus, the anisotropy of transport and magnetic properties of $(La_{0.4}Pr_{0.6})_{1.2}Sr_{1.8}Mn_2O_7$ is probably due to two different factors: (i) the presence of magnetically sensitive Pr atoms having highly anisotropic local susceptibilities and (ii) the changes of the orbital occupancies of the e_g electrons between the $d_{3z^2-r^2}$ and $d_{x^2-y^2}$ orbitals. This shows as well that the role of the rare-earth ion in the substitution of Sr in manganites cannot be reduced to a simple decrease of the average ionic radius of cations. Although it is supposed to control the key parameter of manganites, the magnitude of hopping integral for carriers [16], the presence of magnetically active rare-earth ions in the crystal can also manifest itself in the anisotropy of the physical properties.

We are very grateful to P. J. Brown for her help in using CCSL and for interesting discussions.

[1] *Colossal Magnetoresistive Oxides*, edited by Y. Tokura (Gordon and Breach, New York, 2000).
[2] Y. Moritomo *et al.*, Nature (London) **380**, 141 (1996).
[3] T. Kimura *et al.*, Phys. Rev. Lett. **81**, 5920 (1998).
[4] M. Apostu *et al.*, Phys. Rev. B **64**, 012407 (2001).
[5] I. Gordon *et al.*, Phys. Rev. B **64**, 092408 (2001).
[6] J. Akimitsu *et al.*, J. Phys. Soc. Jpn. **40**, 1621 (1976).
[7] D. N. Argyriou *et al.*, Phys. Rev. B **65**, 214431 (2002).
[8] P. J. Brown and J. C. Matthewman, Cambridge Cristallography Subroutine Library, Rutherford Appleton Laboratory Report No. RAL93-009, 1993.
[9] J. F. Mitchell *et al.*, Phys. Rev. B **55**, 63 (1997).
[10] M. Kubota *et al.*, J. Phys. Soc. Jpn. **69**, 1601 (2000).
[11] D. N. Argyriou *et al.*, Phys. Rev. B **59**, 8695 (1999).
[12] R. J. Papoular *et al.*, Europhys. Lett. **13**, 429 (1990).
[13] M. Takata *et al.*, Acta Crystallogr. Sect. A **50**, 330 (1994).
[14] K. Burger and W. Prandl, Acta Crystallogr. Sect. A **55**, 719 (1999).
[15] A. Gukasov and P. J. Brown, J. Phys. Condens. Matter **14**, 8831 (2002).
[16] S. Okamoto *et al.*, Phys. Rev. B **63**, 104401 (2001).